J Solid State Electrochem (2000) 4: 159–167

ORIGINAL PAPER

K. Suresh Kumar Danadurai · T.M. Sridhar
S.V. Narasimhan · S. Rajeswari

Surface characterisation and crevice corrosion behaviour of nickel-based alloys in the paper industry

Received: 22 February 1999 / Accepted: 6 June 1999

Abstract Recycled water in the paper industry acts as a stronger electrolyte as its concentration and temperature are quite high. The lower pH that exists in these solutions enhances the corrosion and the high concentration of solids leads to leaching of metal ions from surface. Crevice corrosion is a form of localised attack, which can quickly induce metal perforation even with high grade stainless steels like 316L when the protective chromium oxide film is damaged. A specially designed crevice cell assembly was used to study the electrochemical aspects of nickel-based alloys with the commonly used 316L SS. The mounted specimen with its crevice was anodically polarised in a white water medium, which is normally encountered in the paper machine section. The nickel-based alloys show remarkable crevice corrosion resistance. X-ray photoelectron spectroscopy studies revealed that the enhanced corrosion resistance of these alloys is due to the contributing nature of the individual elements Cr, Ni and Mo and their presence in the form of various oxidised species on the passive films.

Key words Nickel-based alloys · Crevice corrosion · White water · Passive films · X-ray photoelectron spectroscopy

Introduction

Corrosion problems in the pulp and paper industries have caused huge losses in terms of repair and replacement. Proper selection of material of construction is very important and serious considerations have to be given in selecting the materials [1]. Crevice corrosion has been observed on a variety of passive film-forming metals exposed to a number of different environments ranging from high purity water to the human body [2]. Crevice corrosion is considered by many to be the most deleterious form of corrosion as it occurs on the shielded areas of a metal surface where it is difficult to examine the underlying metal visually and hence results in unpredicted catastrophic failures [3]. It is the intense localised attack frequency that occurs within crevices or other shielded areas, associated with small volumes of stagnant solution caused by holes, gasket surfaces lap joints, surface deposits and crevices under holes. The corrosion at the wet metal interface is influenced by a number of factors like the composition of the backwater, surface metal and stagnation time. Crevice corrosion is one of the most detrimental forms for stainless steel corrosion in a white water medium [4].

Chloride ions are the most aggressive anions commonly present in a white water system, which replaces the oxygen associated with the passive surface [5]. The concentration of chloride present in white water is also important and varies considerably, depending upon the location of the environment. The practice of closure of the white water system [6, 7] and closed loop operation conditions promotes the accumulation of chloride ions in the suction press roll section and headbox section of the paper mills to alarming proportions, which leads to depletion of oxygen or a reduction in pH within the corroding crevice. Hence, the present study was undertaken to evaluate the crevice corrosion resistance of the nickel-based alloys along with the reference type 316L stainless steel. The nature and composition of the passive films formed on the alloys, which contributed to the enhanced corrosion resistance, were analysed by X-ray photoelectron spectroscopy (XPS).

K. Suresh Kumar Danadurai · T.M. Sridhar · S. Rajeswari (✉)
Department of Analytical Chemistry,
University of Madras, Guindy Campus,
Chennai – 600 025, India
e-mail: raje@uni.mad.ernet.in

S.V. Narasimhan
Water and Steam Chemistry Laboratory,
BARC Facilities, Kalpakkam – 603 102, India

Experimental

The chemical composition of the materials used for the present study were the reference type 316L stainless steel (316L SS) and nickel-based alloys, namely Inconel 825, alloy C-276 and alloy 59 (Table 1). All the specimens were cut into $1 \times 1 \times 0.3$ cm in size from the respective sheet materials. The specimens were soldered to a copper rod for electrical contact and mounted on epoxy-based resin to expose an area of 1 cm^2, which formed the working electrode. The mounted samples were polished using SiC paper up to 800 grit followed by micron diamond paste. The electrodes were ultrasonically cleaned with acetone and rinsed with deionised water.

An electrochemical cell with a capacity of 1000 ml was adopted. The working electrode consisted of stainless steel and nickel-based alloys, with platinum as the counter electrode and SCE as the reference electrode. The electrolyte used was a solution containing chloride, sulfate and thiosulfate to simulate the white water environment, whose composition and operating conditions are given in Table 2. A glass cell assembly designed by Dayal et al. [8] was adopted to determine the crevice corrosion resistance. The features and details of the specially designed crevice cell assembly were as follows. It consisted of a glass assembly to create a crevice on the mounted specimens. The flat tip of the glass rod was brought into close contact with the specimen surface using a nut and thread arrangement. The angle between the glass and the specimen surface was $1.2 \pm 0.2°$. The bulk to crevice area ratio was 5.6 ± 1.5:1. This type of crevice assembly has been found to be very convenient and the mounted specimen with the crevice can be directly used in a standard polarisation cell. The working electrode was then introduced into the cell and the potential was allowed to stabilise for 30 min. The mounted specimen with its crevice assembly was anodically polarised at a scan rate of 1 mV/s from the rest potential in the anodic direction until E_{cc} (the critical crevice potential) was attained where the alloy entered the transpassive region. The specimen surfaces after each experiment were thoroughly examined under an optical microscope, to check the possibility of edge and pitting attack, and any specimens with edge attack and/or pitting attack were rejected. This experimental procedure was followed throughout our investigation.

X-ray photoelectron spectroscopic study

Surface analysis of the passive films using the XPS technique was carried out to understand the nature and composition of the passive films developed on the 316L SS and alloy C-276 samples. The specimens were anodically polarised at 200 mV in the white water solution for a period of 1 h for the growth of the stable passive film. At the end of the experiment the specimens were quickly removed, washed with double distilled water, dried using purified argon and stored in an air-tight desiccator until they were transferred to the vacuum controlled sample chamber of the VG Scientific ESCALAB Mark-II XPS unit for analysis.

The samples were irradiated with Al K_α radiation with a mean energy of 1486.6 eV at a vacuum of 10^{-7}–10^{-9} Torr. The output of the photoelectron spectroscopic analysis was obtained as binding energy versus intensity count plots through a data acquisition system, which was directly interfaced to the XPS unit. For depth profiling of the passive film, an argon ion source attached to the equipment was used at a current of 10–20 μA. The high resolution photoelectron spectra (before and after sputtering) were taken for the $2p_{3/2}$ levels of chromium and nickel and the $3d_{5/2}$ and $3d_{3/2}$ levels of molybdenum. The binding energies of the elements chromium, nickel and molybdenum were measured from the spectra obtained for the respective elements and then the value was corrected with respect to the C 1*s* binding energy. The resolution of the instrument for the Au $4f_{7/2}$ peak with Al K_α was 0.8 eV under the experimental conditions. Data reduction was carried out by deconvoluting the high resolution composite XPS peaks of the individual species of different oxidation states. This was done using PEAKFIT software based on a non-linear regression analysis. Regression models were constructed from the appropriate number of Gaussian peaks with baseline quadratic correction to account for the high binding energy which resulted from the inelastically scattered photoelectrons. The peak position, its intensity and width for each individual Gaussian peak were used as input parameters in deconvoluting the measured spectra. The criteria for the best fit were the minimum chi-square. The final results consisted of the area under each of the resolved peaks for the individual oxidation states, total area under the raw data and total area under the convoluted curve, besides the parameters concerning the resolved peaks. Since curve fitting can provide several solutions to the same spectrum, peak subtraction, double differentiation and measurement of spin-orbit splitting were used to determine the best fit.

Results and discussion

Electrochemical crevice corrosion studies

A series of potentiodynamic anodic polarisation experiments were carried out to determine the crevice corrosion resistance of the nickel alloys compared with the 316L SS reference material in the white water solution using the specially designed crevice assembly. Figure 1 shows the polarisation curve for 316L SS and the nickel alloys in the white water solution. The critical crevice potential (E_{cc}) for 316L SS was +185 mV. Inconel 825 showed a significant improvement in E_{cc} values when compared to the 316L SS. The values of the critical crevice potential for alloy C-276 and alloy 59 are +818 mV and +844 mV, respectively. Alloy C-276 and alloy 59 showed almost immunity towards crevice corrosion. A marginal difference in the E_{cc} was noticed for

Table 2 Chemical composition and operating conditions of the white water solution

Chloride	1000 ppm
Sulfate	1000 ppm
Thiosulfate	50 ppm
pH	3.5
Temperature	55 ± 2 °C

Table 1 Chemical composition of the high performance alloys (wt%)

Material	Cr	Mo	Ni	Fe	Mn	Si	C	N	S
316L	17.3	2.4	12.5	65.3	1.94	0.004	0.030	0.02	0.003
Inconel 825	21.8	3.1	41.7	31.3	0.46	0.200	0.030	–	0.020
Alloy C-276	15.9	16.1	56.8	6.2	0.43	0.040	0.004	–	0.003
Alloy 59	23.2	16.1	59.0	1.0	0.40	0.040	0.005	–	0.003

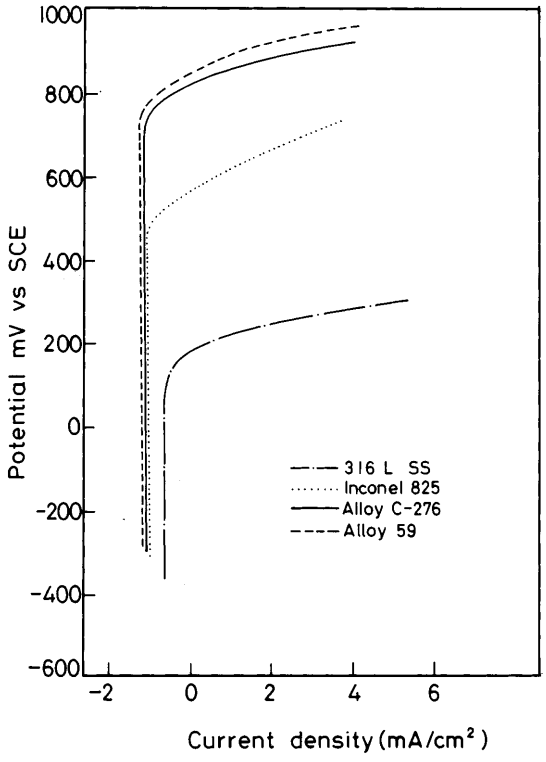

Fig. 1 Potentiodynamic anodic cyclic polarisation curves for 316L SS and nickel-based alloys in the white water medium

alloy C-276 and alloy 59, indicating that the passive films formed on these alloys are stable even in the presence of the crevice.

The mechanism of the crevice is its initiation by de-aeration followed by acidification within the crevice to the point where breakdown of the passive film occurs; this is followed by propagation of the attack [9]. Initially the anodic reaction of slow alloy dissolution and the cathodic oxygen reduction reaction occur both inside and outside the crevice. During this time the oxygen within the crevice is depleted faster than it can be replenished by diffusion and further, the cathodic reaction moves outside the crevice where it can be supported by the higher dissolved oxygen content of the bulk solution. Slowly metal ions concentrate in the crevice and Cl^- ions migrate into the crevice to maintain charge neutrality. Hydrolysis of the metal chloride complexes in the crevice leads to the formation of H^+ ions, lowering the pH of the crevice solution. A point is eventually reached when the metal in the crevice becomes active and the propagation of attack within the crevice ensues. At this stage, rapid dissolution of the metal inside the crevice is driven by the reduction reactions outside the crevice and, if thermodynamically possible, some hydrogen evolution inside the crevice [10].

The build up of the aggressive solution is caused by the passive current flowing within the crevice as the anodic reaction, with oxygen reduction outside the crevice supplying the cathodic reaction. Chromium ions generated by the passive film hydrolyse within the crevice, thereby reducing the pH: mass transport between the anode and the cathode results in ions being carried into the crevice, in this case chloride ions resulting in a fall in the pH and increase in the chloride ion concentration. Eventually the solution becomes severe enough to break down the passive film, thus making 316L SS more prone to crevice attack [10]. The stable passive films formed by the contributing Cr, Ni and Mo alloying elements aid in resisting the crevice attack of these nickel alloys in comparison with 316L SS.

Effect of pH

The pulp and paper industry uses both acid and alkaline paper making processes, but the acidic process is more widely adopted. Typical white water pH is in the range of 4–6 [1, 11]. The pH is controlled on the acid side by alum additions, souring with sulfur dioxide, sulfate or sulfuric acid. As the pH of the white water fluctuates from acidic to near neutral it is necessary to evaluate the performance of the candidate materials in the acidic and neutral (pH 7) conditions.

An improvement in the corrosion resistance was noticed as the acidity of the environment changed to neutral [12]. The crevice corrosion behaviour of 316L SS and the nickel alloys in the white water solution as a function of pH are given in Table 3. The increase in pH of the white water solution (i.e., pH 5 and pH 7.0) resulted in E_{cc} values higher than that at pH 3.5. At the neutral condition there was lack of free H^+ ions, which favours the cathodic reaction corresponding to the reduction of dissolved oxygen present in the environment [8, 13].

$$O_2 + 2H_2O + 4e^- \rightarrow 4OH^-$$

The presence of OH^- ions released by the reduction of oxygen prevents the adsorption of halide ions within the crevice and decreases the propagation by reducing the rate of hydrolysis of MCl [13, 14]. 316L SS exhibited an anodic shift of $+63$ mV in E_{cc} from the white water solution. Alloy C-276 and alloy 59 showed more positive E_{cc} values of $+852$ mV and $+878$ mV, respectively. The breakdown potential becomes more positive as the pH increases, i.e. breakdown is unlikely unless the solution has a very high redox potential. Nickel alloys normally form a protective oxide film in neutral and alkaline solutions, and this is of particular significance for their corrosion resistance.

Effect of temperature

The data on the comparative effect of temperature (28–75 $\pm$ 2 °C) over the crevice corrosion resistance of 316L SS and the nickel alloys in the white water solution are given in Table 4. The results show that at higher temperature an apparent decrease in the crevice corrosion

Table 3 Effect of pH on the crevice corrosion behaviour of modified stainless steels and nickel alloys

Material	pH 3.5		pH 5.0		pH 7.0	
	E_c (mV)	E_{cc} (mV)	E_c (mV)	E_{cc} (mV)	E_c (mV)	E_{cc} (mV)
316L SS	−365	+185	−351	+219	−326	+248
Inconel 825	−322	+556	−332	+595	−329	+620
Alloy C-276	−316	+814	−318	+832	−305	+852
Alloy 59	−310	+840	−304	+860	−294	+878

resistance was noticed for all the alloys. 316L SS exhibited +122 mV active shift in E_{cc} value with a corresponding increase in temperature from 28 to 75 ± 2 °C. The E_{cc} values in the white water solution at 75 ± 2 °C were 802 mV and 825 mV, respectively, for alloy C-276 and alloy 59.

It is reported [15] that crevice corrosion increases with an increase in the temperature of the solution. Moreover, the presence of halide ions in the bulk of the solution gives access to the crevice area, which results in a higher concentration of halide ions within the crevice and acceleration of crevice corrosion, but the nickel alloys offer good resistance even under these conditions. The performance of the nickel alloys is attributed to the stable nature of the passive films formed on the surface and hence the films formed on alloy C-276 and 316L SS were characterised by XPS.

XPS analysis of the passive films of the nickel alloys

XPS analysis was carried out to understand the composition and contributing nature of the individual elements and their presence in the form of various oxidised species on the passive film of the alloys, which revealed relatively better and superior corrosion resistance. The passive film consists of mainly oxides and hydroxides, and its thickness in many cases is only a few atomic layers. The corrosion behaviour of stainless steel is dependent on the properties of the passive film. The composition of these passive films is determined by the composition of the alloy as well as by the environment to which the alloy is exposed. The main elements that contribute towards the formation of such barriers are chromium, molybdenum, nickel, nitrogen, etc. In order to ascertain the factors controlling the chemical composition and the stability of these metallic oxides in the passive film, it is essential to discuss the role played by these elements. By using surface sensitive techniques like XPS, also known by the corresponding acronym "ESCA", it is possible to obtain information about the composition of very thin reaction products formed on the surfaces.

Cr $2p_{3/2}$ spectra

The high-resolution XPS spectra of the Cr $2p_{3/2}$ energy level was recorded in the binding energy window 560–600 eV for 316L SS and alloy C-276 passive films and is shown in Fig. 2. Deconvolution of the Cr $2p_{3/2}$ energy level for 316L SS yielded four peaks. The peaks at binding energy values of 576.1, 577.1 and 579.2 eV correspond to Cr_2O_3, $CrOOH/Cr(OH)_3$ and CrO_4^{2-}, respectively. The metal peak at a binding energy value of 574.4 eV is almost negligible in comparison with the amplitudes of the other peaks (Table 5). The intensity of these components are in the order of $Cr(OOH)/Cr(OH)_3 > CrO_4^{2-} > Cr_2O_3 \gg Cr$. This indicates that the outermost layer of the passive film contains $Cr(OH)_3$ as the major constituent. The intensities of the Cr $2p_{3/2}$ levels were nearly doubled on sputtering with argon. The feature change is the enrichment of the Cr_2O_3 phase at the inner layer and the complete vanishing of the CrO_4^{2-} peak. The intensity of the Cr_2O_3 peak increases from 0.25 (25% of Cr_2O_3 in the outermost layer) to 0.46 (46% of Cr_2O_3 in the innermost layers) on sputtering, indicating that Cr_2O_3 is present in the inner layer of the passive films, i.e. at the metal oxide interface.

XPS analysis of Cr $2p_{3/2}$ for alloy C-276 alloy differs from 316L SS. The Cr $2p_{3/2}$ binding energy and composition are illustrated in Table 6. In alloy C-276 the Cr_2O_3 composition in the passive film is 46% while the ion sputtered surface showed only 34%. For the sputtered surface the composition of $Cr(OH)_3$ also decreases from 35% to 30% for the sputtered surface. This illustrates that Cr_2O_3 is mainly present in the outermost layer and $Cr(OH)_3$ is present in the inner layers for the nickel alloy. In all the above cases, chromium was found as Cr^{3+} and Cr^{6+} in various forms of oxides and hy-

Table 4 Effect of temperature on the crevice corrosion behaviour of modified stainless steels and nickel alloys

Material	28 ± 2 °C		55 ± 2 °C		75 ± 2 °C	
	E_c (mV)	E_{cc} (mV)	E_c (mV)	E_{cc} (mV)	E_c (mV)	E_{cc} (mV)
316L SS	−334	+252	−365	+185	−325	+130
Inconel 825	−285	+597	−345	+556	−334	+504
Alloy C-276	−278	+835	−332	+814	−326	+802
Alloy 59	−272	+860	−320	+840	−318	+825

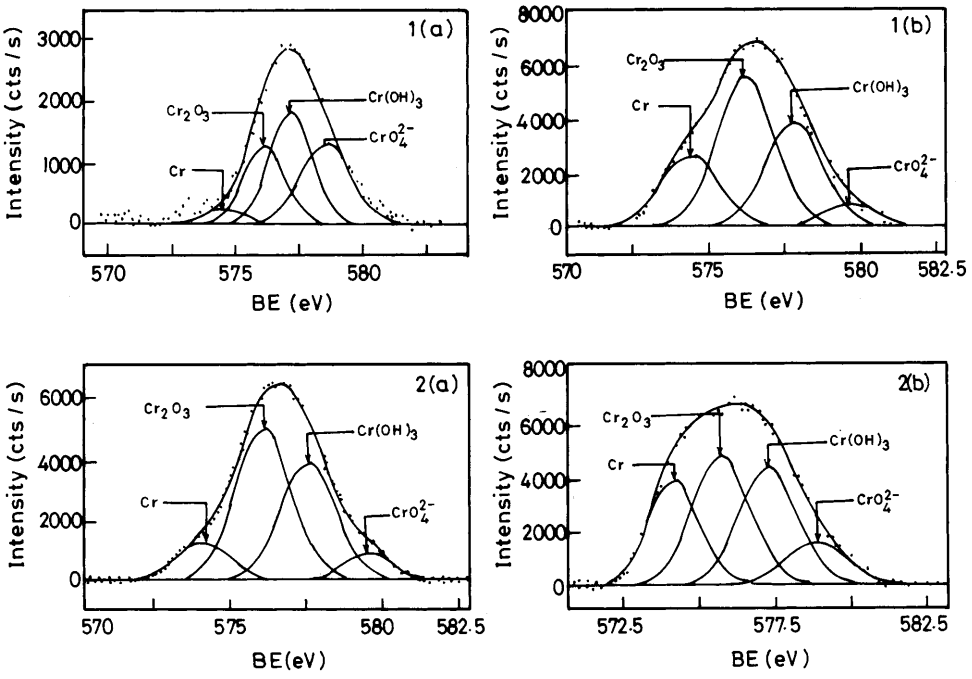

Fig. 2 High resolution XPS spectra of chromium in the passive film of **a** the passivated surface and **b** the sputtered surface for **1** 316L SS and **2** alloy C-276

Table 5 Binding energy (eV), intensity values (counts s^{-1}) and relative quantities of various chromium species for 316L SS

Sample	BE (eV)	Intensity (counts/s)	Proposed species
Passivated surface			
	574.4	455.5	Cr
	576.1	2512.6	Cr_2O_3
	577.1	3786.2	$Cr(OH)_3$
	579.2	3118.5	CrO_4^{2-}
Cr/(total intensity)		0.0461	
Cr_2O_3/(total intensity)		0.2545	
$Cr(OH)_3$/(total intensity)		0.3835	
CrO_4^{2-}/(total intensity)		0.3159	
Sputtered surface			
	574.4	4266.9	Cr
	576.2	10883.7	Cr_2O_3
	577.8	7060.1	$Cr(OH)_3$
	579.6	1215.8	CrO_4^{2-}
Cr/(total intensity)		0.1821	
Cr_2O_3/(total intensity)		0.4646	
$Cr(OH)_3$/(total intensity)		0.3014	
CrO_4^{2-}/(total intensity)		0.0519	

Table 6 Binding energy (eV), intensity values (counts s^{-1}) and relative quantities of various chromium species for Alloy C-276

Sample	BE (eV)	Intensity (counts/s)	Proposed species
Passivated surface			
	574.1	2603.3	Cr
	576.1	11326.9	Cr_2O_3
	577.6	8642.2	$Cr(OH)_3$
	579.6	1586.9	CrO_4^{2-}
Cr/(total intensity)		0.1078	
Cr_2O_3/(total intensity)		0.4688	
$Cr(OH)_3$/(total intensity)		0.3577	
CrO_4^{2-}/(total intensity)		0.0657	
Sputtered surface			
	574.1	7989.2	Cr
	575.7	11052.0	Cr_2O_3
	577.2	10008.4	$Cr(OH)_3$
	579.0	3739.7	CrO_4^{2-}
Cr/(total intensity)		0.2437	
Cr_2O_3/(total intensity)		0.3371	
$Cr(OH)_3$/(total intensity)		0.3052	
CrO_4^{2-}/(total intensity)		0.1141	

droxides at their respective binding energy values, which are in agreement with earlier reports [16–18].

Ni $2p_{3/2}$ spectra

The specimens were scanned between 850.0 eV and 865.0 eV to study the $2p_{3/2}$ energy levels of nickel and its oxidation states in the passive film. The deconvoluted high-resolution spectra are illustrated in Fig. 3. A very weak signal for Ni $2p_{3/2}$ with a count rate of less than 400 counts s^{-1} was observed for the 316L SS sample. This is obviously due to the small amount of nickel present in the chemical composition of the bulk sample. However, this envelope could be deconvoluted into three contributions at binding energies 852.8, 854.4 and 855.4 eV for the passive films. The intensity of the peaks was doubled on sputtering for 10 min with argon ions (Fig. 3). The peak at 852.8 eV is reported to be due to metallic nickel present underneath the passive film [19–21]. The other two contributions at 854.4 eV and 855.4 eV are reported to be due to the nickel species NiO and $Ni(OH)_2$. The metal ion contribution is increased from 52% to 58% on sputtering with argon ions. On the

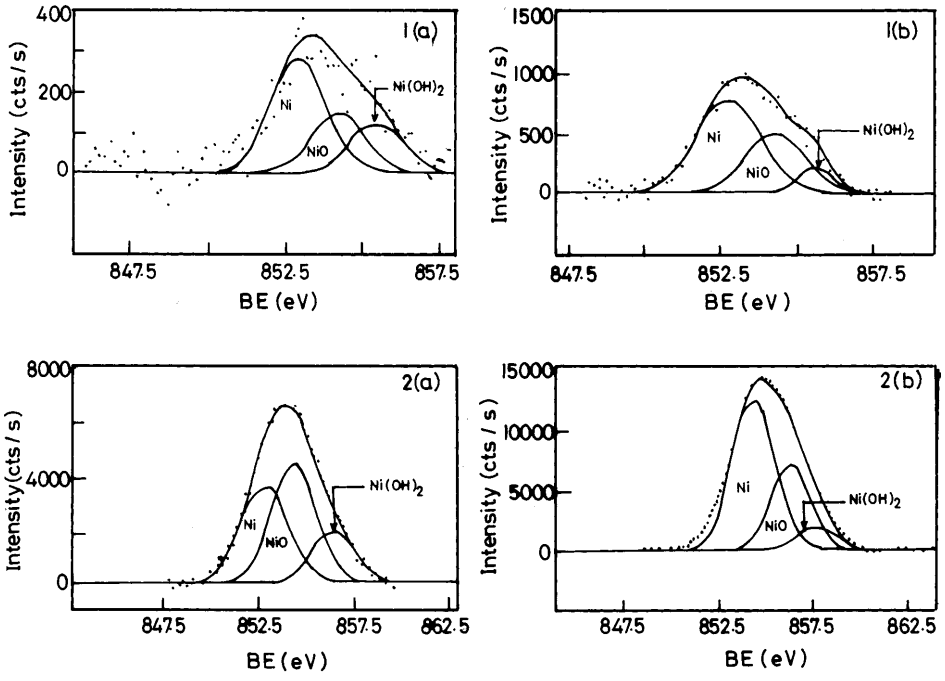

Fig. 3 High-resolution XPS spectra of nickel in the passive film of **a** the passivated surface and **b** the sputtered surface for **1** 316L SS and **2** alloy C-276

other hand, the NiO contribution increases from 26% to 34% while the hydroxide component drastically decreases from 22% to 8%.

Alloy C-276 showed prominent Ni $2p_{3/2}$ signals with high intensity due to the very high percentage of nickel in the alloy. The envelope could be deconvoluted into three components at binding energy values of 852.8, 854.3 and 856.3 eV for Ni metal, NiO and $Ni(OH)_2$, respectively. After sputtering the peak due to the metal increases while the peak due to the $Ni(OH)_2$ constituent decreases.

Mo 3d spectra

Molybdenum, as an alloying element, is known for its role in improving the passivation properties and corrosion resistance of stainless steels [22, 24]. The Mo 3*d* energy levels were analysed in the binding energy region between 235 and 240 eV to identify the presence of molybdenum and its oxides in the passive films. The molybdenum 3*d* spectra are very complex owing to the fact that the signal is a doublet, Mo $3d_{5/2}$ and Mo $3d_{3/2}$, and that various oxidation states exist in the oxide products. Deconvolution of the spectrum for different oxidation states was made with the imposed condition that the Mo $3d_{5/2}$ and Mo $3d_{3/2}$ energy levels are separated by 3.1 eV and their intensity ratio is 3:2, respectively, according to the theoretical predictions [25]. The deconvoluted high-resolution spectra of Mo 3*d* are illustrated in Fig. 4.

A very weak signal with a count rate around 600 counts s^{-1} was observed for the passive films of the 316L SS specimen. The Mo 3*d* spectrum was deconvoluted into two components for Mo and Mo^{4+} at respective binding energies of 227.7, 228.7 and 230.5 for the presence of Mo, MoO_2 and MoO_4^{2-} species. After argon sputtering the intensity of the metallic peak increases drastically compared to its Mo^{4+} oxide.

Mo 3*d* peaks with very high oxide intensities were observed for alloy C-276. The 3*d* envelope was deconvoluted for four contributions. Apart from Mo, Mo^{4+} and Mo^{6+}, another set of peaks at 233.0 and 236.0 eV were observed. These peaks may be due to some intermetallic molybdenum species, as proposed earlier [26]. After sputtering, the oxides were almost removed and the Mo^{4+} oxide remains separate from the metal.

XPS studies of passive films formed on Fe-Cr alloys and stainless steels have indicated that a chromium-rich film is responsible for maintaining passivity [16]. Furthermore, it was also suggested that the Cr-rich film consists of the hydrated form of CrOOH [17, 27]. Studies by Olefjord and Marcus [20], however, suggest that Cr_2O_3 is the main passivity compound. The presence of the chromium-rich phase suggests the direct reaction of chromium with water to form Cr_2O_3 and perhaps some CrO_3, followed by formation of $Cr(OH)_3$ at the oxide-solution interface. These reactions constitute the initial passivation process. Brooks et al. [16] reported that the passive film consists of a Cr-rich inner layer. The Cr-rich film contains a non-crystalline Cr_2O_3 film and traces of CrO_3. Highly hydrated amorphous $Cr(OH)_3$ in water is also formed. This phase deprotonates and recrystallises during passivation.

It has been reported that CrO_4^{2-} anions may be formed in the solid state by reaction of $Cr(OH)_3$ with OH^- in the lattice [16]. Hence

$$Cr(OH)_3 + 5OH^- \rightarrow CrO_4^{2-} + 4H_2O + 3e^-$$

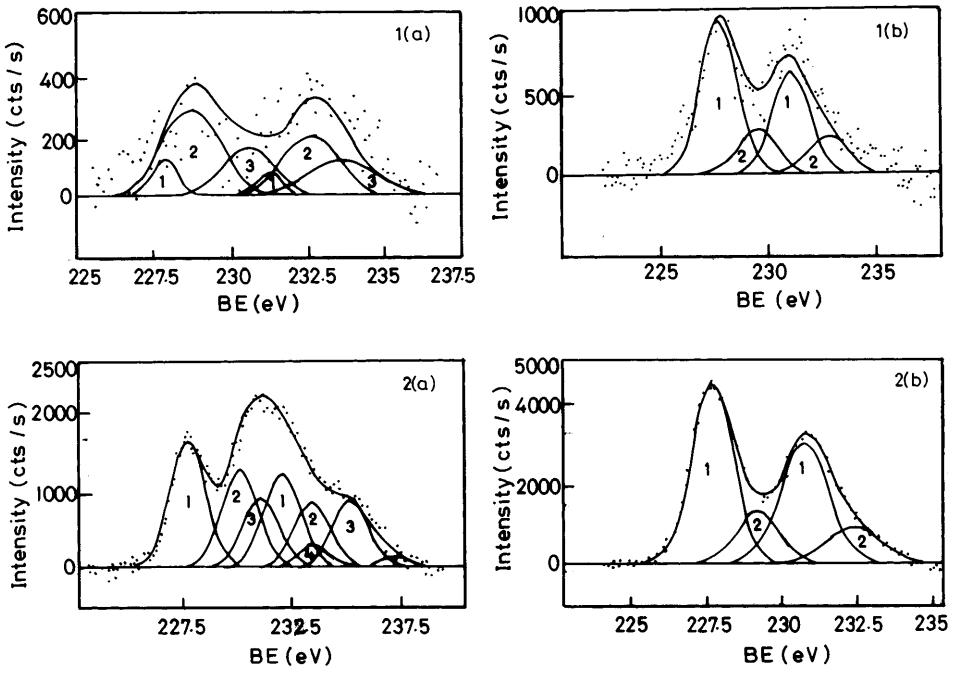

Fig. 4 High-resolution XPS spectra of molybdenum in the passive film of **a** the passivated surface and **b** the sputtered surface for **1** 316L SS and **2** alloy C-276. The deconvoluted peaks are **1** MO, **2** MoO_2, **3** MoO_4^{2-} and **4** $MoNi_4$

It is possible that CrO_4^{2-} species form insoluble salts in the $Cr(OH)_3$ layers. The presence of CrO_4^{2-} and MoO_4^{2-} is not expected since both the ions are unstable at lower pH. However, it is reported in the literature that they are formed in the solid state by reaction of lower-valent metallic ions with lattice-trapped water in the gel-like disordered state at the onset of passivity and Brooks et al. [16] clearly discuss the formation of CrO_4^{2-}. The solid state environment of Cr^{3+} in the gel would be suitably enriched with OH^- anions and lattice water to enable the formation of CrO_4^{2-}. It is also suggested that the solid state environment of Cr^{3+} ions in the gel would be suitably enriched with OH^- ions and lattice water to enable the formation of CrO_4^{2-}.

It has been pointed out [28] that anions of the type MO_4^{n-} which inhibit corrosion may act as electron acceptors, resulting in the reduction in electrical conductivity and increase in M-O bond strengths of the film in which they are incorporated. The report also reveals that CrO_4^{2-} ions are able to operate at full capacity as anodic inhibitors at a surface coverage as low as 4%, which is just above the detection limit of XPS. The formation of Cr-O bonds leads to a stronger passive film. The deprotonation reaction may take the following course [29]:

$$Cr(OH)_3 \xrightarrow{-H_2O} CrOOH \xrightarrow{-H_2O} Cr_2O_3$$

The growth of the Cr_2O_3 layer at the passive film is accomplished by the above transformation. Thus, Cr_2O_3 is formed at the metal-film interface by oxygen anion migration to the metal surface. The presence of chromium oxide barrier layers is the primary means of passivation and the incorporation of CrO_4^{2-} bipolarises the passive film and thus enhances the deprotonation process, leading to further growth in the barrier layer as well as impeding the ingress of OH^- and Cl^- ions [16].

The presence of Cr^{3+} at the binding energy value of 576 eV in the form of Cr_2O_3 was identified in the outermost layer and also on the sputtered surface. In the case of alloy C-276 the peak intensities for Cr_2O_3 were found to be higher. Previous reports suggested that the presence of Cr_2O_3 is beneficial in increasing the localised corrosion resistance, as the hydroxide ions reduce the defects in the passive film [30]. Therefore the presence of Cr_2O_3 with higher magnitude could have enhanced the corrosion resistance of the alloys whereas the magnitude of Cr_2O_3 was found to be lower in reference material 316L SS, thus accounting for the lower corrosion resistance.

For 316L SS the signal emitted by metallic nickel is intense, which ultimately shows that the hydroxide or oxide of the nickel film on the surface is extremely thin. No significant peak for Ni^{2+} oxide is detected. However, intense peaks for Ni^{2+} oxide and hydroxide were observed for C-276.

In recent studies it was reported that metallic nickel underneath the passive film was enriched during anodic polarisation [31, 32] and it was speculated that nickel may contribute to passivation and improved pitting resistance through the formation of intermetallic bonds with Cr and Mo and that this reduces anodic dissolution. Halada et al. [33] explained the enrichment of Cr and retention of Ni in the alloy surface layer just beneath the passive film. It was reported that the formation of a molybdenum-nickel intermetallic phase of the type $MoNi_4$ and its strong Mo-Ni intermetallic bond was the driving force for the enrichment of Mo and Ni during polarisation. The intermetallic layer along with the passive film enriched the source of the oxide-forming

metallic species directly beneath the passive film and hence may be responsible for the outstanding stability against localised corrosion attack of the nickel alloys [21].

Enrichment of nickel and molybdenum amounting to 19.4–27% of Ni and 3.5–6% of Mo beneath the passive film is noted for Fe-20% Cr-20% Ni-6% Mo alloys. Such an enrichment accounts for a compositional ratio of nickel to molybdenum of 4.7. The Engel-Brewer [26] theory of intermetallic bonding supports the occurrence of such enrichment as a result of the formation of an intermetallic compound of the type $MoNi_4$. In our study, the Ni and Mo content of the nickel alloys are considerably higher. Hence, according to the Engel-Brewer theory, the possibility of formation of $MoNi_4$ is very high. XPS results proved the formation of this intermetallic compound. The anodic segregation of nickel and molybdenum may be driven by the energy state of the intermetallic phase formed by selective dissolution. The stability of these surface phases for a given environment and the role of alloying elements on the stability of passive films needs further study.

Lu et al. [34] pointed out that Mo could form Mo^{6+} oxide in the passive film, thereby blocking the penetration of Cl^-. An almost defect-free oxide layer is formed in which ionic conductivity is low. At higher anodic potentials, insoluble MoO_4^{2-} that blocks active dissolution may form, as long as stable metal species are available to bind to the MoO_4^{2-} [35]. The enhanced production of MoO_4^{2-} may be a result of an increase in pH at the passive film-solution interface. XPS analysis, however, indicated that the addition of Mo to the alloy tended to increase the proportion of Cr_2O_3 compared to $Cr(OH)_3$ and Mo^{4+} with Cr_2O_3 being enriched at the metal-film interface. Thus, Mo tends to promote the formation of an oxide rather than hydroxide based film. MoO_4^{2-} was found by XPS to be enriched in the outer layer with CrO_4^{2-}. The higher content of nickel and molybdenum strongly shifts the anodic polarisation curve towards the more noble direction and reduces the (local) dissolution current, the acidification of the pit embryo and thus facilitates repassivation. The combination of these facts explains the outstanding resistance against localised corrosion of the nickel alloys compared to the reference type 316L SS.

Conclusions

The reference material 316L SS was found to be highly susceptible to crevice attack in the paper machine white water environment. A remarkable crevice corrosion resistance was observed for nickel-based alloys. Alloy C-276 and alloy 59 exhibit superior performance in this medium. With the increase in pH and temperature, the crevice corrosion resistance was found to be improved on comparison with 316L SS. The increased resistance to crevice attack exerted by nickel alloys can be attributed to the stabilisation of the passive films formed on the surface by the specific alloying elements Cr, Ni and Mo, as revealed by XPS results. The passive layer contains Cr_2O_3 in the inner layers and $Cr(OH)_3$ as the major constituent in the outermost layer. The presence of Mo and its oxides further establishes its role in increasing the corrosion resistance. The nickel concentration beneath the passive layer was also found to be increased due to anodic segregation, which can aid intermetallic compound formation. This intermetallic layer, along with the passive film enriched with stable MoO_4^{2-} species, resulted in reduced anodic dissolution, providing an enriched source of oxide-forming metallic species directly beneath the passive film and hence improvement in the corrosion resistance of the nickel alloys.

Acknowledgements One of the authors (K.S.K.D) acknowledges the CSIR, New Delhi, for financial assistance and Dr. Santhanu Bera, WSCL, BARC facilities, Kalpakkam, for his help in acquiring XPS data.

References

1. Wensley DA (1987) Paper machine corrosion. In: ASM Handbook: Corrosion. American Society for Metals, Metals Park, Ohio, pp 13: 1186–1190
2. Shaw BA, Moran PJ, Gartland P (1993) Crevice corrosion of a nickel-based super alloy in natural and chlorinated seawater. In: Proceedings of the 12th International corrosion congress, vol. 3B. NACE, Houston, pp 1915–1927
3. Shreir LL, Jarman RA, Burstein (1994) Corrosion metal/environmental reactions. Butterworth-Heinemann, London
4. Bowers DF, McFarland T (1984) Tappi J 67: 86
5. Muhonen JM (1974) Pulp and paper industry corrosion problems. NACE, Houston, p 75
6. Geller A, Gottsching L (1982) Tappi J 65: 97
7. Bowers DF (1978) Tappi J 61: 57
8. Dayal RK, Parvathawarthani N, Gnanamoorthy JB (1983) Br Corros J 18: 184
9. Oldfield JW, Sutton WH (1978) Br Corros J 13: 13
10. Oldfield JW, Sutton WH (1980) Br Corros J 15: 31
11. Garner A (1984) J Pulp Paper Sci 10: J51
12. Leckie HP, Uhlig HH (1966) J Electrochem Soc 113: 1261
13. Fontona MG (1987) Corrosion engineering. McGraw-Hill, Singapore
14. Heubner U, Rocbel M, Wallis F (1989) Werkst Korros 40: 40
15. Hibner EL, Ross RW (1983) Corrosion/83. NACE, Houston, p 163
16. Brooks AR, Clayton CR, Doss K, Lu YC (1986) J Electrochem Soc 133: 2459
17. Sugimoto K, Sawada Y (1977) Corros Sci 17: 425
18. Childs PE, Laub LW, Wagner JB (1971) Proc Br Ceram Soc 19: 21
19. Halada GP, Clayton CR, Herman H (1995) J Electrochem Soc 142: 74
20. Olefjord I, Marcus P (1982) Surf Interface Anal 4: 23
21. Rossi A, Elsener B (1993) XPS study of passive films on stainless steel in neutral solutions. In: Proceedings of the 12th International corrosion congress, vol 3B. NACE, Houston, pp 2120–2130
22. Tullin C, Jungstrom EL (1989) Energy Fuels 3: 284
23. Johnson O (1975) Chem Scr 8: 162
24. Asami K, Hashimoto K, Shimodaira S (1976) J Jpn Inst Metals 40: 438
25. Grunert W, Stakheev AY, Feldhans R, Anders K, Sphire ES, Mnachev KM (1991) J Phys Chem 95: 1323

26. Brewer L (1968) Science 161: 115
27. Asami K, Hashimoto K, Masumoto T, Shimodaira S (1976) Corros Sci 16: 909
28. Rozenfiled IL (1981) Corrosion inhibitors. McGraw-Hill, New York
29. Sakashita M, Sato N (1978) Bipolar fixed charge induced passivity. In: Frankenthal RP, Kruger J (eds) Passivity of metals. The Electrochemical Society, Pennington, NJ, p 479
30. Dobbellaar JAL, deWit JHW (1990) J Electrochem Soc 137: 2038
31. Clayton CR, Castle JE (1977) Corros Sci 17: 1
32. Olefjord I, Olfstrom B (1977) In: Hoar TP (ed) Proceedings of the 6th European Congress on Metallic Corrosion. Society of Chemical Industry, London, p 21
33. Halada GP, Kim D, Clayton CR (1996) Corrosion 52: 36
34. Lu YC, Ives MB, Clayton CR (1993) Corros Sci 35: 89
35. Newman RC (1985) Corros Sci 25: 341